Applied Physics Letters ARTICLE scitation.org/journal/apl

Charge transport mechanism in SiN_x-based memristor

Cite as: Appl. Phys. Lett. **115**, 253502 (2019); doi: 10.1063/1.5127039
Submitted: 8 September 2019 · Accepted: 5 December 2019 ·
Published Online: 19 December 2019

A. A. Gismatulin,[1] V. A. Gritsenko,[1,2,3] T.-J. Yen,[4] and A. Chin[4,a)]

AFFILIATIONS

[1]Rzhanov Institute of Semiconductor Physics SB RAS, 13 Lavrentiev Ave., 630090 Novosibirsk, Russia
[2]Novosibirsk State University, 2 Pirogov Str., 630090 Novosibirsk, Russia
[3]Novosibirsk State Technical University, 20 Marx ave., 630073 Novosibirsk, Russia
[4]Department of Electronics Engineering, National Chiao Tung University, Hsinchu 300, Taiwan

[a)]Author to whom correspondence should be addressed: achin@nctu.edu.tw

ABSTRACT

Amorphous silicon nitride is a key dielectric in silicon devices. The advantage of SiN_x and Si_3N_4 over other dielectrics is that silicon nitride is compatible with silicon technology and is widely used in it. It is necessary to understand, experimentally and theoretically, the mechanism of charge transport in a memristor based on silicon nitride in the initial, high-resistance, and low-resistance states to develop a resistive memory element. At present, there is currently no single universal model of charge transport in a memristor based on silicon nitride. In our work, the charge transport of the initial, high, and low resistive states in an SiN_x-based memristor is analyzed with four bulk-limited charge transport models. It is established that the Frenkel model of Coulomb traps ionization, Hill-Adachi model of overlapping Coulomb traps, and Makram-Ebeid and Lannoo model of multiphonon isolated traps ionization, quantitatively, do not describe the charge transport of the SiN_x-based memristor in any state. The Nasyrov-Gritsenko model of phonon-assisted tunneling between traps gives a consistent explanation of the charge transport of the SiN_x-based memristor in all states at temperatures above room temperature.

Currently, the driving force in microelectronics is universal memory development, which combines high speed and an infinite number of RAM reprogramming cycles, nonvolatility and high information capacity of flash memories, and hard drive low cost. The attempts in developing a universal memory are ongoing. At present, the following physical nonvolatile memories are being intensively studied: resistive (memristor[1,2]) memory (Resistive Random Access Memory, ReRAM), chalcogenide-based phase transition memory, magnetoresistive memory, and ferroelectric memory. Different types of nonvolatile memories have their advantages and disadvantages. One of the most promising candidates for a universal memory is considered to be a memristor based on the reversible transition of a dielectric film from a high resistance state (HRS) to a low resistance state (LRS) and back when a current pulse is applied.[3,4] Now, it is generally accepted that the transition to the LRS occurs due to the filament (a thin conductive nanowire with a diameter of 1–5 nm) formation.[5] The small filament size opens up a possibility of developing a resistive memory matrix with the design norm of 5 nm, which corresponds to a terabit scale memory.[6]

The memristor has two important promising practical applications. The first application is associated with the use of a memristor as a high-speed, nonvolatile, and radiation-resistant matrix of a flash memory that stores information when the power is off. Another important practical application of memristors is their use in the embedded memory of microcontrollers. The second promising use of memristors is associated with using them as an active element in neuromorphic cognitive systems to simulate the work of a biological element—a synapse—in modeling the brain work.[7] Recently, there have also been several reports of artificial neurons based on diffusive memristors.[8,9]

The memristor effect is observed in a wide class of different materials: $SrTiO_3$-type perovskite films, organic films,[10] high-k dielectrics (TiO_2, HfO_2,[11] ZrO_2, Ta_2O_5,[12] TaO_x,[13,14] Ta_2O_{5-x}/TaO_{2-x},[15] Nb_2O_5, and Al_2O_3), oxides (SiO_x[16–18] and GeO_x),[19] and nitrides (SiN_x and SiO_xN_y) of silicon and germanium.[20–22]

Amorphous SiO_x and SiN_x are two key dielectrics in silicon devices. The advantage of SiN_x and Si_3N_4[20–22] over other dielectrics is that silicon nitride is compatible with the silicon technology and is widely used in it.[23,24] Another advantage is the large bandgap Si_3N_4 value $E_g = 4.6$ eV. On the one hand, this leads to low leakage currents of this material. On the other hand, silicon enrichment allows controlling the

physical properties of SiN_x in a wide range, which opens up the possibility of optimizing the storage properties of memristors based on Si_3N_4 and SiN_x. The advantage of Si_3N_4 and SiN_x over SiO_2 is their higher atomic density, higher chemical stability and, in particular, high oxidation resistance. It can be expected that, due to the lower nitrogen diffusion coefficient in silicon nitride,[25] compared with the oxygen diffusion coefficient in silicon oxide,[26] the storage time of the memristor information (limited by the diffusion of nitrogen or oxygen vacancies) based on silicon nitride will be longer than the storage time of the memristor information based on silicon oxide.

Despite numerous studies,[20,22,27–31] there is currently no single universal model of charge transport in a memristor based on silicon nitride. The aim of this work is to study, experimentally and theoretically, the mechanism of charge transport in a memristor based on silicon nitride in the initial, high-resistance, and low-resistance states.

The Ni/SiN_x/p^+-Si ReRAM devices were made on a highly doped p-type (p^+) Si substrate. Then, the 20 nm thick SiN_x was formed by Plasma Enhanced Chemical Vapor Deposition (PECVD) using silane (SiH_4) and NH_3 with the N_2 carrier gas. The deposition temperature was 300 °C, and such low temperature is needed for integrating into the backend of the integrated circuit. The 50 nm thick Ni was deposited on the SiN_x film by electron beam evaporation with an area radius of 60 um. The current-voltage (*IV*) characteristics were measured by the HP 4155B Semiconductor Parameter Analyzer.

The current of the SiN_x-based structure at a voltage of about 10 V abuts against the instrument current limitation of 300 μA and in reverse the voltage sweep; it remains in this current limitation to about 0.6 V. Therefore, at 10 V, the structure switched to another resistance. When the sweep to negative voltages is in the region of −2 V, a sharp drop in current occurs by an order of magnitude, and during reverse sweeping, the current value becomes less. After that, when sweeping to the positive voltage at 4 V, the current rises sharply and remains at the same value during a further sweep. Consequently, the SiN_x-based structure exhibits typical memristor properties, such as the forming process and bipolar resistance switching [Fig. 1(a)]. The endurance and retention of the memristor show that a SiN_x-based structure not only exhibits memristor properties but also retains them for at least 10^4 resistance switching cycles [Fig. 1(b)].

To clarify the charge transport mechanism, the temperature *IV* characteristics were taken in the memristor state before the forming process—Virgin State (VS)—in the HRS and LRS. These characteristics were compared with four bulk models: the Frenkel model, Hill-Adachi model, Macram-Ebeid and Lannoo model, and Nasyrov-Gritsenko model.

The current I through the material containing traps can be described by the expression[14,27]

$$I = eN^{2/3}SP. \tag{1}$$

Here, e is electron charge, $N = s^{-3}$ is trap concentration, s is average distance between traps, S is contact area, and P is trap ionization probability.

The Frenkel effect consists in lowering the Coulomb potential of an isolated Coulomb trap under the influence of an applied electric field. The trap ionization probability by the Frenkel effect is described by the expression[28,29]

$$P = \nu \exp\left(-\frac{W - \beta_F\sqrt{\frac{U}{d}}}{kT}\right), \quad \beta_F = \left(\frac{e^3}{\pi\varepsilon_\infty\varepsilon_0}\right)^{1/2}. \tag{2}$$

Here, $\nu = W/h$ is attempt to escape factor, W is trap ionization energy, h is the Plank constant, β_F is the Frenkel constant, U is voltage, d is thickness, k is the Boltzmann constant, T is temperature, e is electron charge, ε_∞ is high frequency permittivity, and ε is dielectric constant.

The Frenkel effect simulating the experimental data of the SiN_x-based memristor in all states is presented in Table I. The trap energy W is determined from the temperature dependence of the *IV* characteristic. The attempt to escape factor $\nu = W/h$ is determined from the ionization energy. The selection parameters are the trap concentration N and high-frequency permittivity ε_∞. The typical dielectric trap concentration range is 1×10^{18} to 1×10^{22} cm^{-3}.[30,31] The experimentally obtained value using ellipsometry high-frequency permittivity is $\varepsilon_\infty = n^2 = 4$. When simulating the Frenkel effect in all memristor states, the abnormally low trap concentrations and the abnormally big high-frequency dielectric constant value in the range of 9–19 are obtained. Therefore, the Frenkel model does not describe the SiN_x-based memristor charge transport mechanism in any state.

The overlapping Coulomb trap Hill-Adachi (H-A) model takes into account, at a small distance between traps, the overlap neighboring trap integral and the trap interaction in an electric field (Table I). The trap ionization probability, in this case, is described by the expression[32,33]

$$P = 2\nu \exp\left(-\frac{W - \frac{e^2}{\pi\varepsilon_\infty\varepsilon_0 s}}{kT}\right) \sinh\left(\frac{e\frac{U}{d}s}{2kT}\right). \tag{3}$$

The H-A model qualitatively describes the charge transport in the SiN_x-based memristor in all states at reasonable values of trap concentrations, trap energies, and high-frequency permittivity (Table I).

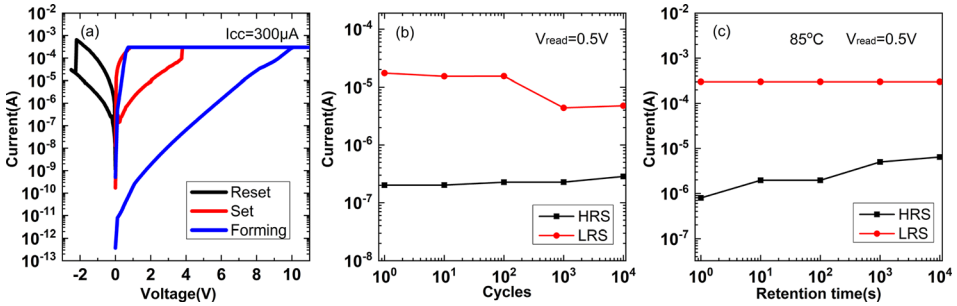

FIG. 1. (a) Experimental current-voltage characteristics of the RRAM based on SiN_x. (b) Endurance of the memristor at room temperature. Pulse width = 1 us, $V_{set} = 7$, and $V_{reset} = -7$ V. (c) Retention of the memristor at 85 °C in HRS and LRS states.

TABLE I. Model parameters summary (red indicates the nonphysical model parameters).

	Frenkel model	H-A model	ME-L model	N-G model
VS	$N = 1.4 \times 10^{11}$ cm^{-3}	$N = 3.6 \times 10^{19}$ cm^{-3}	$N = 1 \times 10^{15}$ cm^{-3}	$N = 3.6 \times 10^{19}$ cm^{-3}
	$W = 0.7$ eV	$W = 1.05$ eV	$m^* = 0.7\ m_e$	$m^* = 0.17\ m_e$
	$\nu = 1.7 \times 10^{14}$ s^{-1}	$\nu = 2 \times 10^{8}$ s^{-1}	$W_t = 0.6$ eV	$W_t = 1.2$ eV
	$\varepsilon_\infty = 9$	$\varepsilon_\infty = 4$	$W_{opt} = 1.2$ eV	$W_{opt} = 2.4$ eV
HRS	$N = 1 \times 10^{17}$ cm^{-3}	$N = 1 \times 10^{20}$ cm^{-3}	$N = 1.5 \times 10^{20}$ cm^{-3}	$N = 1 \times 10^{20}$ cm^{-3}
	$W = 0.62$ eV	$W = 1.2$ eV	$m^* = 1.75\ m_e$	$m^* = 0.06\ m_e$
	$\nu = 1.5 \times 10^{14}$ s^{-1}	$\nu = 6.9 \times 10^{11}$ s^{-1}	$W_t = 0.53$ eV	$W_t = 1.2$ eV
	$\varepsilon_\infty = 19$	$\varepsilon_\infty = 4$	$W_{opt} = 1.06$ eV	$W_{opt} = 2.4$ eV
LRS	$N = 8.3 \times 10^{17}$ cm^{-3}	$N = 1 \times 10^{20}$ cm^{-3}	$N = 1.4 \times 10^{21}$ cm^{-3}	$N = 1 \times 10^{20}$ cm^{-3}
	$W = 0.58$ eV	$W = 1.2$ eV	$m^* = 1.75\ m_e$	$m^* = 0.05\ m_e$
	$\nu = 1.4 \times 10^{14}$ s^{-1}	$\nu = 2.1 \times 10^{13}$ s^{-1}	$W_t = 0.48$ eV	$W_t = 1.08$ eV
	$\varepsilon_\infty = 16$	$\varepsilon_\infty = 4$	$W_{opt} = 0.96$ eV	$W_{opt} = 2.16$ eV

At the trap energy $W = 1.05$ eV in the VS, the attempt to escape factor has a value $\nu = W/h = 2.5 \times 10^{14}$ s^{-1} and at the trap energy $W = 1.2$ eV in the HRS and LRS, the attempt to escape factor has a value $\nu = W/h = 2.9 \times 10^{14}$ s^{-1}.[21] However, the H-A predicts a small attempt to escape factor value from $\nu = 2 \times 10^{8}$ s^{-1} in the VS to $\nu = 2.1 \times 10^{13}$ s^{-1} in the LRS. Therefore, the H-A model does not describe the charge transport in an SiN_x-based memristor in any state.

The Makram-Ebeid and Lannoo (ME-L) multiphonon model of isolated trap ionization describes the charge transport in the case when an electron in the trap is ionized by absorbing the energy of several phonons, tunnels into the conduction band, moves through the electric field and is captured by an neighboring trap. This process is repeated until the electron reaches the opposite contact (Table I). Such ionization probability is described by the formula[34]

$$P = \sum \exp\left(\frac{nW_{ph}}{2kT} - \frac{W_{opt} - W_t}{W_{ph}} \coth\frac{W_{ph}}{2kT}\right) \times I_n\left(\frac{W_{opt} - W_t}{W_{ph}\sinh\left(W_{ph}/2kT\right)}\right) P_i(W_t + nW_{ph}),$$
$$P_i = \frac{e\left(\frac{U}{d}\right)}{2\sqrt{2m^* W}} \exp\left(-\frac{4}{3}\frac{\sqrt{2m^*}}{\hbar e\left(\frac{U}{d}\right)} W^{3/2}\right). \quad (4)$$

Here, W_t is thermal trap energy, W_{opt} is optical trap energy W_{ph} is phonon energy, I_n is the modified Bessel function, P_i is tunneling probability through a triangular barrier, m^* is electron effective mass, m_e is electron mass, and $\hbar$ is the Plank constant.

The ME-L model describes the *IV* characteristics of the SiN_x-based memristor only in strong fields (Table I). For the VS, the ME-L model predicts a low trap concentration $N = 1 \times 10^{15}$ cm^{-3}, which is not typical of dielectrics (the dielectric trap concentration range is 1×10^{18} to 1×10^{22} cm^{-3}[30,31]) and it predicts the large trap concentration $N = 1.5 \times 10^{20}$ cm^{-3} in the HRS and $N = 1.4 \times 10^{21}$ cm^{-3} in the LRS. At such high trap concentrations, the distance between the traps becomes small, and the ME-L model is transformed into the Nasyrov-Gritsenko model (N-G).

The N-G model of phonon-assisted tunneling between neighboring traps describes the charge transport when the distance between the traps is small and, after the trap ionization, it is more beneficial for the charge to immediately tunnel to the neighboring trap without entering the conduction band [Fig. 2(a)]. The range of the trap concentration limit for the N-G model is $N = 5 \times 10^{18}$ to 5×10^{21} cm^{-3}. At a trap concentration value lower than $N = 5 \times 10^{18}$ cm^{-3}, an electron cannot tunnel to a neighboring trap, and it tunnels to the conduction band (ME-L model). A metallic conductivity is observed at trap concentrations higher than $N = 5 \times 10^{21}$ cm^{-3} due to tunneling between traps. N-G ionization probability is described by the expression[35]

$$P = \frac{2\sqrt{\pi}\hbar W_t}{m^* s^2 \sqrt{2kT(W_{opt} - W_t)}} \exp\left(-\frac{W_{opt} - W_t}{kT}\right) \times \exp\left(-\frac{2s\sqrt{2m^* W_t}}{\hbar}\right) \sinh\left(\frac{e\frac{U}{d}s}{2kT}\right). \quad (5)$$

The N-G model describes the *IV* characteristics of the SiN_x-based memristor in all states [Fig. 2(a)]. At the trap concentration of $N = 3.6 \times 10^{19}$ cm^{-3}, thermal trap energy $W_t = 1.2$ eV, and optical trap energy $W_{opt} = 2.4$ eV, the N-G model predicts the effective electron mass $m^* = 0.17\ m_e$ in the VS. The trap energies are obtained from the temperature dependence of *IV* characteristics. In the HRS, in which the filament is almost completely ruptured, the charge transport goes along the same traps as in the VS state, where there is no filament at all. Therefore, the trap energies in these states are the same. The presence of a partially ruptured filament in the N-G model is explained by an increase in the trap concentration. In the LRS, the number of traps remains the same as in the HRS, but since the charge transport is determined through the conductive filament, the trap energy becomes different. However, the N-G model in HRS and LRS predicts small effective masses $m^* = 0.06\ m_e$ and $m^* = 0.05\ m_e$, respectively. When simulating the charge transport through the SiN_x-based memristor, we set the electric field distribution to be linear, although with a high trap concentration this is not always true. Consequently, we associate small effective masses, neglecting the local electric field distribution in the structure. In addition, the differences between experimental and model characteristics at low voltages in the VS are explained by the fact that the voltage sweep is a dynamic process, but the N-G simulation is a static model. To obtain more accurate effective

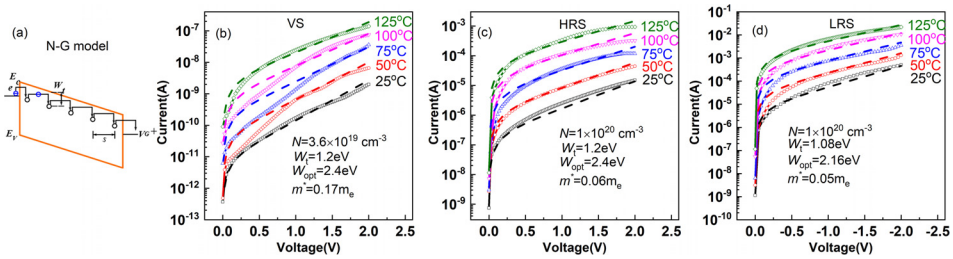

FIG. 2. (a) Schematic representation of the N-G model. Experimental current-voltage characteristics of the RRAM based on SiN_x in (b) VS, (c) HRS, and (d) LRS state and the simulation data by the N-G model.

mass values and to take into account dynamic process at a low voltage, it is necessary to solve the Poisson equation when taking into account the Shockley-Reed-Hall trap occupation statistics. In addition, when deriving the analytical formula of the N-G model from a numerical expression, the following limits were introduced: $kT \ll W_t$ and $(eUs)/d < W_t/4$.[35] From these limitations for the LRS case, it turns out that the temperature should be less than 10^4 K and the voltage is less than 10 V.

In conclusion, four bulk-limited models were applied to the simulation of the experimental charge transport of the SiN_x-based memristor in various states. The Frenkel model of isolated Coulombic trap ionization predicts too small trap concentration values for SiN_x. In addition, the Frenkel model gives the fitting parameter of the high frequency dielectric permittivity in HRS and LRS, which is too big for an SiN_x structure. The Hill-Adachi model of overlapping Coulombic centers quantitatively explains the slope in the charge transport of the SiN_x-based RRAM in the HRS but predicts the small attempt to escape factor in all states. The ME-L multiphonon model predicts a low trap concentration value in the VS and a high trap concentration values in the HRS and LRS. Therefore, the ME-L model gives the trap concentration value beyond the model applicability range. The N-G model of phonon-assisted electron tunneling between nearby traps described the charge transport in the SiN_x-based memristor with a reasonable trap concentration and trap energies. However, the N-G model gives small effective electron mass values in the HRS and LRS, which can be clarified when solving the Poisson equation with the Shockley-Read-Hall statistics for trap occupation.

Fabrication of experimental samples and the experiments were carried out jointly by a grant of the Russian Science Foundation (Project № 18-49-08001) and by the Ministry of Science and Technology (MOST) of Taiwan (Project № 107-2923-E-009-001-MY3). The experimental data simulation was carried out with the support of the Russian Foundation for Basic Research (RFBR) (Project № 19-29-03018). We are grateful to D. R. Islamov for the discussions.

REFERENCES

[1]L. O. Chua and S. M. Kang, Proc. IEEE **64**(2), 209–223 (1976).
[2]J. J. Yang, M. D. Pickett, X. M. Li, D. A. A. Ohlberg, D. R. Stewart, and R. S. Williams, Nat. Nanotechnol. **3**(7), 429–433 (2008).
[3]M. A. Zidan, J. P. Strachan, and W. D. Lu, Nat. Electron. **1**(1), 22–29 (2018).
[4]M. Terai, Y. Sakotsubo, S. Kotsuji, and H. Hada, IEEE Electron Device Lett. **31**(3), 204–206 (2010).
[5]L. Vandelli, A. Padovani, L. Larcher, G. Broglia, G. Ori, M. Montorsi, G. Bersuker, and P. Pavan, inIEEE International Electron Devices Meeting (IEDM) (2011).
[6]J. M. Tour, G. Wang, Y. Yang, and Y. Ji, U.S. Patent No. 9,997,705 B2 (2018).
[7]C. Wu, T. W. Kim, H. Y. Choi, D. B. Strukov, and J. J. Yang, Nat. Commun. **8**, 752 (2017).
[8]Z. R. Wang, S. Joshi, S. Savel'ev, W. H. Song, R. Midya, Y. N. Li, M. Y. Rao, P. Yan, S. Asapu, Y. Zhuo, H. Jiang, P. Lin, C. Li, J. H. Yoon, N. K. Upadhyay, J. M. Zhang, M. Hu, J. P. Strachan, M. Barnell, Q. Wu, H. Q. Wu, R. S. Williams, Q. F. Xia, and J. J. Yang, Nat. Electron. **1**(2), 137–145 (2018).
[9]R. Midya, Z. Wang, S. Asapu, X. Zhang, M. Rao, W. Song, Y. Zhuo, N. Upadhyay, Q. F. Xia, and J. J. Yang, Adv. Intell. Syst. **1**(7), 1900084 (2019).
[10]A. A. Minnekhanov, A. V. Emelyanov, D. A. Lapkin, K. E. Nikiruy, B. S. Shvetsov, A. A. Nesmelov, V. V. Rylkov, V. A. Demin, and V. V. Erokhin, Sci Rep. **9**, 10800 (2019).
[11]H. Y. Lee, P. S. Chen, T. Y. Wu, Y. S. Chen, C. C. Wang, P. J. Tzeng, C. H. Lin, F. Chen, C. H. Lien, and M. J. Tsai, in International Electron Devices Meeting (2008), p. 297.
[12]Z. Wei, Y. Kanzawa, K. Arita, Y. Katoh, K. Kawai, S. Muraoka, S. Mitani, S. Fujii, K. Katayama, M. Iijima, T. Mikawa, T. Ninomiya, R. Miyanaga, Y. Kawashima, K. Tsuji, A. Himeno, T. Okada, R. Azuma, K. Shimakawa, H. Sugaya, I. Takagi, R. Yasuhara, K. Horiba, H. Kumigashira, and M. Oshima, in International Electron Devices Meeting (2008), p. 293.
[13]T. V. Perevalov, V. A. Gritsenko, A. A. Gismatulin, V. A. Voronkovskii, A. K. Gerasimova, V. S. Aliev, and I. A. Prosvirin, Nanotechnology **29**(26), 264001 (2018).
[14]V. A. Gritsenko, T. V. Perevalov, V. A. Voronkovskii, A. A. Gismatulin, V. N. Kruchinin, V. S. Aliev, V. A. Pustovarov, I. P. Prosvirin, and Y. Roizin, ACS Appl. Mater. Interfaces **10**(4), 3769–3775 (2018).
[15]M. J. Lee, C. B. Lee, D. Lee, S. R. Lee, M. Chang, J. H. Hur, Y. B. Kim, C. J. Kim, D. H. Seo, S. Seo, U. I. Chung, I. K. Yoo, and K. Kim, Nat. Mater. **10**(8), 625–630 (2011).
[16]A. A. Gismatulin, V. N. Kruchinin, V. A. Gritsenko, I. P. Prosvirin, T. J. Yen, and A. Chin, Appl. Phys. Lett. **114**(3), 033503 (2019).
[17]T. J. Yen, A. Gismatulin, V. Volodin, V. Gritsenko, and A. Chin, Sci. Rep. **9**, 6144 (2019).
[18]A. Mehonic, A. L. Shluger, D. Gao, I. Valov, E. Miranda, D. Ielmini, A. Bricalli, E. Ambrosi, C. Li, J. J. Yang, Q. F. Xia, and A. J. Kenyon, Adv. Mater. **30**(43), 1801187 (2018).
[19]A. V. Shaposhnikov, T. V. Perevalov, V. A. Gritsenko, C. H. Cheng, and A. Chin, Appl. Phys. Lett. **100**(24), 243506 (2012).
[20]S. Kim, H. Kim, S. Hwang, M. H. Kim, Y. F. Chang, and B. G. Park, ACS Appl. Mater. Interfaces **9**(46), 40420–40427 (2017).
[21]M. N. Koryazhkina, S. V. Tikhov, A. N. Mikhaylov, A. I. Belov, D. S. Korolev, I. N. Antonov, V. V. Karzanov, O. N. Gorshkov, D. I. Tetelbaum, P. Karakolis, and P. Dimitrakis, J. Phys.: Conf. Ser. **993**, 012028 (2018).
[22]S. V. Tikhov, A. N. Mikhaylov, A. I. Belov, D. S. Korolev, I. N. Antonov, V. V. Karzanov, O. N. Gorshkov, D. I. Tetelbaum, P. Karakolis, and P. Dimitrakis, Microelectron. Eng. **187–188**, 134–138 (2018).
[23]V. A. Gritsenko, in *Thin Films on Si: Electronic and Photonic Applications*, edited by V. Narayanan, M. Frank, and A. A. Demkov (World Scientific Press, 2016), pp. 273–322.
[24]V. A. Gritsenko, T. V. Perevalov, O. M. Orlov, and G. Y. Krasnikov, Appl. Phys. Lett. **109**(6), 062904 (2016).
[25]K. Kijima and S. Shirasaki, J. Chem. Phys. **65**(7), 2668–2671 (1976).
[26]J. J. Perez-Bueno, R. Ramirez-Bon, Y. V. Vorobiev, F. Espinoza-Beltran, and J. Gonzalez-Hernandez, Thin Solid Films **379**(1–2), 57–63 (2000).

[27]D. R. Islamov, V. A. Gritsenko, and A. Chin, Optoelectron. Instrum. Data Process. **53**(2), 184–189 (2017).
[28]J. Frenkel, Tech. Phys. USSR **5**(8), 685–695 (1938).
[29]J. Frenkel, Phys. Rev. B **54**, 647 (1938).
[30]F. L. Hampton and J. R. Cricchi, Appl. Phys. Lett. **35**(10), 802–804 (1979).
[31]K. A. Nasyrov and V. A. Gritsenko, Phys-Usp. **56**(10), 999–1012 (2013).
[32]R. M. Hill, Philos. Mag. **23**(181), 59–86 (1971).
[33]H. Adachi, Y. Shibata, and S. Ono, J. Phys. D: Appl. Phys. **4**(7), 988–994 (1971).
[34]S. S. Makram-Ebeid and M. Lannoo, Phys. Rev. B **25**, 6406 (1982).
[35]K. A. Nasyrov and V. A. Gritsenko, J. Appl. Phys. **109**(9), 093705 (2011).